

# Three-stage binarization of color document images based on discrete wavelet transform and generative adversarial networks

Yu-Shian Lin<sup>1†</sup>, Rui-Yang Ju<sup>1†</sup>, Chih-Chia Chen<sup>1</sup>, Ting-Yu Lin<sup>2</sup> and Jen-Shiun Chiang<sup>1\*</sup>

<sup>1</sup>Department of Electrical and Computer Engineering, Tamkang University, No.151, Yingzhuang Rd., Tamsui Dist., New Taipei City, 251301, Taiwan.

<sup>2</sup>Department of Engineering Science, National Cheng Kung University, No. 1 University Rd., East Dist., Tainan City, 70101, Taiwan.

\*Corresponding author(s). E-mail(s): [jsken.chiang@gmail.com](mailto:jsken.chiang@gmail.com);

Contributing authors: [abcpp12383@gmail.com](mailto:abcpp12383@gmail.com); [jryjry1094791442@gmail.com](mailto:jryjry1094791442@gmail.com);  
[crystal88irene@gmail.com](mailto:crystal88irene@gmail.com); [tonylin0413@gmail.com](mailto:tonylin0413@gmail.com);

<sup>†</sup>These authors contributed equally to this work.

## Abstract

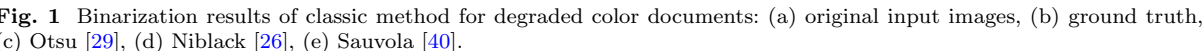
The efficient segmentation of foreground text information from the background in degraded color document images is one of the most critical issues in the ancient document preservation tasks. Due to the imperfect preservation of ancient documents over a long period of time, various types of degradation, including staining, yellowing, and ink seepage, have seriously affected the results of image binarization. In this work, a three-stage method is proposed for image enhancement and binarization of degraded color document images by using discrete wavelet transform (DWT) and generative adversarial networks (GAN). In Stage-1, we use DWT and retain the LL subband images to achieve the image enhancement. In Stage-2, the original input image is split into four (Red, Green, Blue and Gray) single-channel images, each of which is trained by the independent adversarial networks. The trained adversarial network models are employed to extract the color foreground information from the images. In Stage-3, in order to combine global and local features, the output image from Stage-2 and the original input image are employed to train the independent adversarial networks for document binarization. The experimental results demonstrate that our proposed method outperforms many classical and state-of-the-art (SOTA) methods on the Document Image Binarization Contest (DIBCO) datasets. We have released our implementation code at <https://github.com/abcpp12383/ThreeStageBinarization>.

**Keywords:** semantic segmentation, discrete wavelet transform, handwritten document image binarization, document enhancement, handwriting text recognition, generative adversarial networks

## 1 Introduction

The study of historical human society has been conducted mainly through the reconstruction and analysis of preserved ancient documents.

Throughout the development of human society, important ancient documents have been preserved mainly through parchment manuscripts and paintings. The challenge in analyzing preserved ancient documents is that preserved documents are often



With the development of deep learning techniques, neural networks have been applied to image binarization methods. Calvo-Zaragoza and Gallego [4] proposed a selectional auto-encoder approach to parse the text through a trained network model and binarize the text using thresholds. Fully Convolutional Network (FCN) [23, 31] enables the generated images to maintain the same size as the input images, and the task of generating document binarization using FCN [47] is also included in the semantic segmentation task. Hsia

To evaluate the performance of the proposed method for degraded document image binarization, we tested different methods for comparison

on DIBCO datasets of 2011, 2013, 2014, 2016, 2017, and 2018 [28, 33, 35–38].

This paper has the following contributions: (1) A three-stage method is proposed for the first time to perform image enhancement and binarization on degraded color documents. (2) Using DWT before training the GAN can improve the model performance with better balance of text detail extraction and background error suppression. (3) The proposed method achieves SOTA performance on multiple benchmark datasets.

## 2 Related Work

In the past research on document image binarization, the methods can be generally classified into two categories: traditional image processing methods and semantic segmentation methods based on deep learning. Traditional image processing binarization methods are initially based on the calculation of pixel-level local threshold values of images, including global binarization methods [29] and local adaptive binarization methods [26, 40]. However, the traditional image processing binarization methods are not satisfactory for processing documents with excessive interference or degradation.

With the development of deep learning technology, the convolutional neural network (CNN) framework [20, 49] has become the main backbone of computer vision tasks. Semantic segmentation [23] is one of the most important research directions in computer vision, and document image binarization is included in the semantic segmentation task. Tensmeyer *et al.* [47] combined P-FM and FM loss training FCN to apply the model to the document image binarization task. Ronneberger *et al.* [39] improved FCN and proposed U-Net, which uses a U-shaped network architecture to obtain contextual and location information. Peng *et al.* [30] were inspired to add an encoder-decoder architecture to the document image binarization, by which the decoder maps the low-resolution representation to the original size to obtain the binarized image. Vo *et al.* [48] first applied hierarchical deep supervised network (DSN) to document image binarization and achieved the SOTA performance on several benchmark datasets. He *et al.* [11] proposed an iterative deep learning framework applied to document

image binarization and the trained model achieved excellent performance.

In recent years, GAN [8] has achieved exciting results [19, 43] in generating real-world images. Unlike GAN [8] which generates output images from random noises, Isola *et al.* [14] proposed Pix2Pix GAN based on conditional GAN (cGAN) [24] for image-to-image translation. To ensure that the generated images are more realistic, Pix2Pix GAN uses generators to train loss functions. In the network architecture, the generator compares the minimized generated image with the expected output image and measures the  $L1$  loss between them, while the discriminator determines the trustworthiness of the generated image based on the input image and the target image. The operation is shown in the following equation:

$$\begin{aligned} \arg \min_G \max_D V(G, D) = & \mathbb{E}_x[\log(1 - D(x, G(x)))] \\ & + \mathbb{E}_{x,y}[\log D(x, y)] + \lambda \mathbb{E}_{x,y}[\|y - G(x)\|_1] \end{aligned} \quad (1)$$

where the input data distribution  $\mathbb{P}_x$  samples the input image  $x$ ; the ground truth image of the input image is  $y$ , and the hyperparameter to increase the model regularization effect is  $\lambda$ . Generator  $G$  generates the input image as the generated image  $G(x)$ . From Eq. (1), the loss function between the generated image and the ground truth image is  $L1$  instead of  $L2$ , which is beneficial to reduce the blurring and ambiguity in the generation process.

Bhunia *et al.* [3] performed texture enhancement on the dataset and used cGAN [24] for image binarization. Inspired by Pix2Pix GAN [14], Zhao *et al.* [50] proposed a cascade generator structure for document image binarization based on Pix2Pix GAN to solve the problem of multi-scale information combination. De *et al.* [5] designed two discriminators to combine local and global information. Suh *et al.* [42] set up a two-stage generative adversarial network for image binarization using Patch GAN [14]. Nicolaou *et al.* [27] proposed the TorMentor image enhancement framework by adapting global image enhancement transformations to continuous local transformations using plasma fractals. Souibgui *et al.* [41] proposed a new encoder-decoder architecture based on visual converters for enhancing machine printed and handwritten document images. These

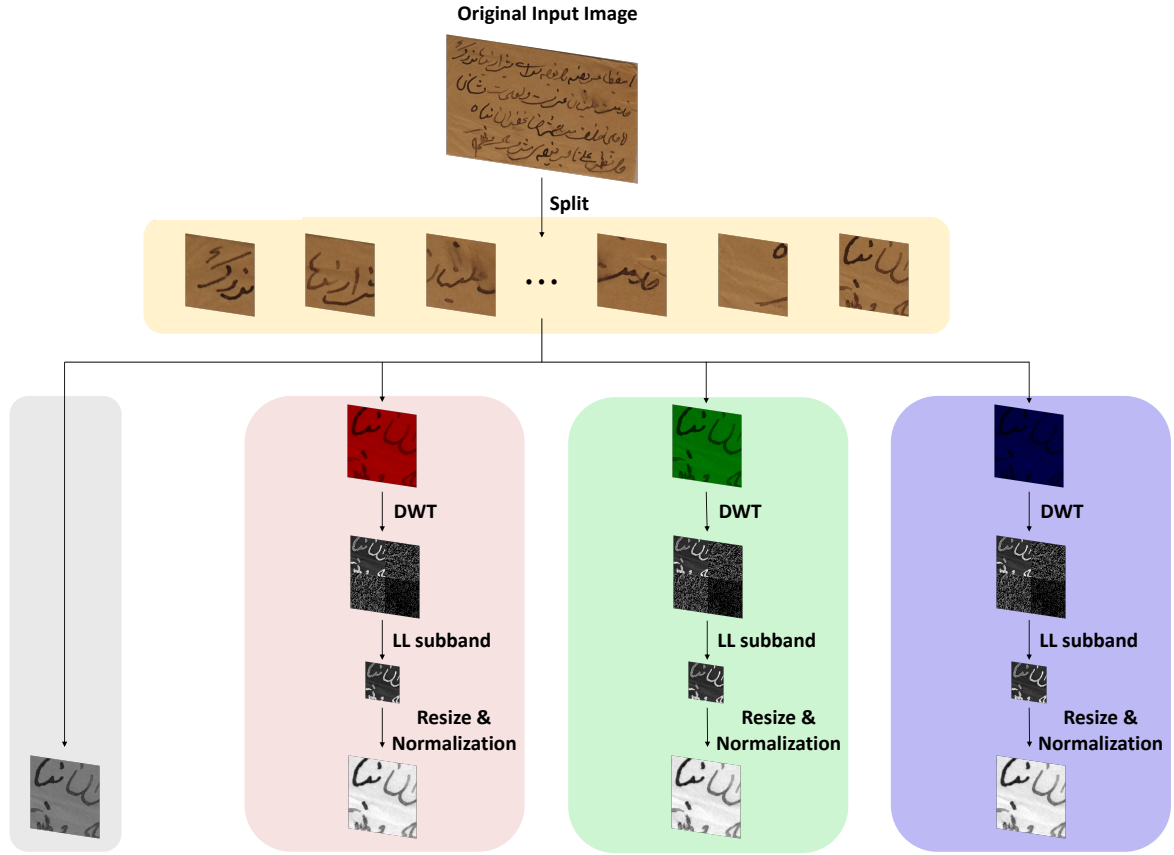


**Fig. 2** Flowchart of Stage-1 in our method.

methods keep breaking the SOTA performance on DIBCO datasets.

### 3 Proposed Method

#### 3.1 Overall Network Architecture

Our goal is to perform image enhancement on degraded color documents and extract text information from the document images. Since the degradation of color document images is diverse and complex, which requires processing of images with different color channels, our proposed method divides the overall network architecture into three stages. In Stage-1, we retain the image of LL subband by DWT, which is prepared for Stage-2 and Stage-3 to train the ground truth image of the generator in the adversarial network. Stage-2 is to remove background color noise and extract color foreground information, and Stage-3 is to perform document binarization to

obtain the final output. The three stages operate independently, and the specific contents of each stage are introduced in Sections 3.2, 3.3, and 3.4 respectively.

#### 3.2 Stage-1

For color document images, this study uses four independent generators to extract foreground color information and remove the image background color. We split the input color image into four single-channel images (red, green, blue, and gray). While the target mask image (Ground Truth, GT) provided by the dataset is a grayscale binary image with only one channel (0 for character pixel points and 1 for background pixel points). The images with different channel numbers cannot be directly input to the discriminator for processing. Therefore, in Stage-1, we first split the three channels (red, green, blue, RGB) of the original input image to form single-channel images of



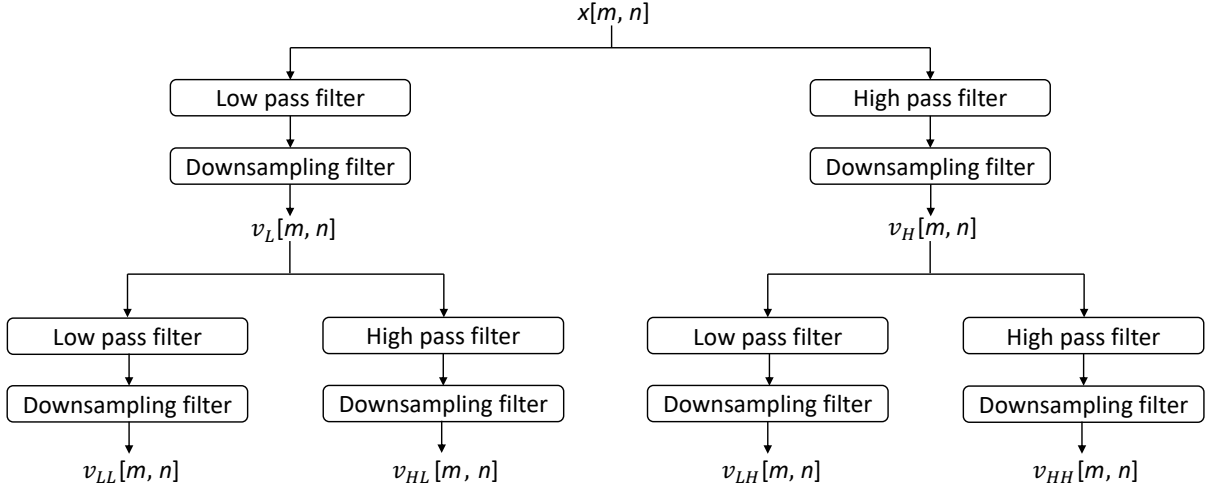


**Fig. 3** Flowchart of discrete wavelet transform calculations.

RGB, then perform DWT on each of the RGB single-channel images and retain the LL subband images for normalization. The target mask images and the output images of Stage-1 are used as the corresponding ground truth images of the generators in RGB and gray channels. Fig. 2 shows the flowchart of Stage-1, splitting the image into three single-channel RGB images for DWT, then retaining the LL subband images, and resizing them to a specific size ( $224 \times 224$ ).

### 3.2.1 Discrete Wavelet Transform

Discrete Wavelet Transform (DWT) is the inner product of the original image with the wavelet basis function and scale function, which can be regarded as a bandpass filter, allowing only signals with frequencies similar to the wavelet basis function to pass through. Fig. 3 shows the flowchart of discrete wavelet conversion. When the input signal is  $x[m, n]$ , we first process the  $n$ -direction as high pass, low pass, and frequency reduction to get an image with low frequency composition on the left and high frequency composition on the right. The equation for the one-dimensional DWT is shown below:

$$\begin{aligned}
 v_L[m, n] &= \sum_{k=0}^{K-1} x[m, 2n - k]g[k] \\
 v_H[m, n] &= \sum_{k=0}^{K-1} x[m, 2n - k]h[k]
 \end{aligned} \tag{2}$$

We can perform high-pass, low-pass, and frequency reduction for Eq. (2) extended in the  $m$ -direction to obtain the following equations:

$$\begin{aligned}
 v_{LL}[m, n] &= \sum_{k=0}^{K-1} v_L[2m - k, n]g[k] \\
 v_{HL}[m, n] &= \sum_{k=0}^{K-1} v_L[2m - k, n]h[k]
 \end{aligned} \tag{3}$$

$$\begin{aligned}
 v_{LH}[m, n] &= \sum_{k=0}^{K-1} v_H[2m - k, n]g[k] \\
 v_{HH}[m, n] &= \sum_{k=0}^{K-1} v_H[2m - k, n]h[k]
 \end{aligned} \tag{4}$$

The image after DWT operation is divided into four subbands, one low frequency subband and three high frequency subbands, respectively. As shown in Fig. 4, they are LL subband in the upper left corner, HL subband in the upper right corner, LH subband in the lower left corner, and HH subband in the lower right corner.

Unlike the target mask images provided by the dataset, the single-channel images produced by the original input images may have a lot of noises, which cannot be directly used as the corresponding ground truth images in the generator, and that may affect the trained adversarial network. The DWT would decompose the image to

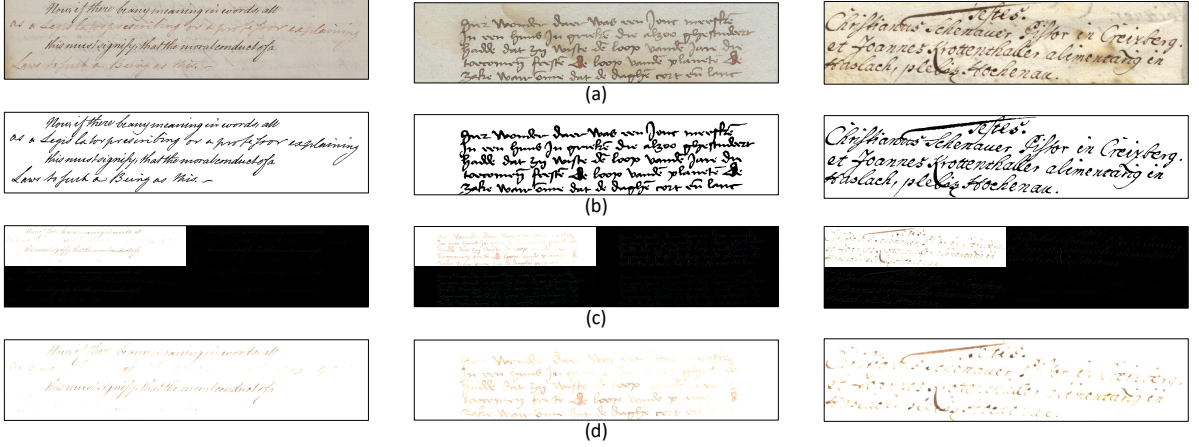


**Fig. 4** Examples of DWT of images in the DIBCO dataset; (a) the original input image, (b) the ground truth, (c) 2-D Discrete Wavelet Transform, (d) the image of LL subband.

get low-frequency information and high-frequency information, where the low-frequency information corresponds to the mean value and the high-frequency information corresponds to the difference value. The mean value is the local average value and belongs to the low-frequency information, which changes slowly and stores the picture contour information and approximate information. While the difference value is the local fluctuation value and belongs to the high-frequency information, which changes faster and stores the picture detail information and local information (containing noises). Therefore, we perform DWT and retain the LL subband images as the corresponding ground truth images, which have achieved the effect of storing contour information and noise reduction.

### 3.2.2 Normalization

Normalization is the process of limiting the data to the desired range in order to facilitate the subsequent processing of the data and to speed up the convergence, and the equation is as shown:

$$I_N = (IV_{\text{nmax}} - IV_{\text{nmin}}) \frac{1}{1 + e^{-\frac{I-\beta}{\alpha}}} + IV_{\text{nmin}} \quad (5)$$

where  $IV$  is the intensity values, the image to be processed  $I : \{\mathbb{X} \subseteq \mathbb{R}^n\} \rightarrow \{IV_{\text{min}}, \dots, IV_{\text{max}}\}$ , and the generated image  $I_N : \{\mathbb{X} \subseteq \mathbb{R}^n\} \rightarrow \{IV_{\text{nmin}}, \dots, IV_{\text{nmax}}\}$ .  $\alpha$  defines the width of the

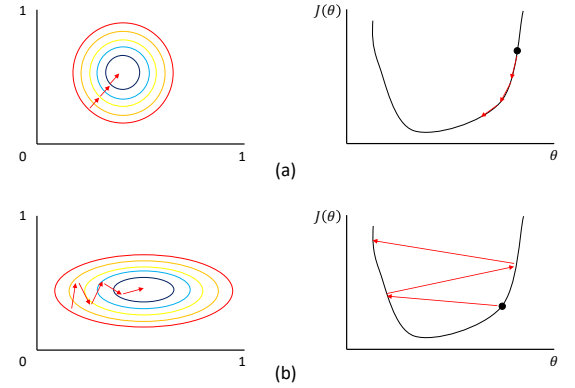


**Fig. 5** (a) The pixel value size distribution of the RGB components is similar. (b) The pixel value size distribution of the RGB components is not similar.

input intensity range, and  $\beta$  defines the range centered intensity.

The input image is a color document image, and the image is composed of red, blue, and green components. When the pixel values of the RGB components in the document image are distributed similarly and no pixel value of a component is too large or too small, the gradient update trajectory of the model is more stable, reliable, and fast, as shown in Fig. 5 (a). However, due to the complexity and diversity of the degraded color document images, the pixel value size distribution of the RGB components is not similar. The practical situation may be that the first document image in the dataset is dominated

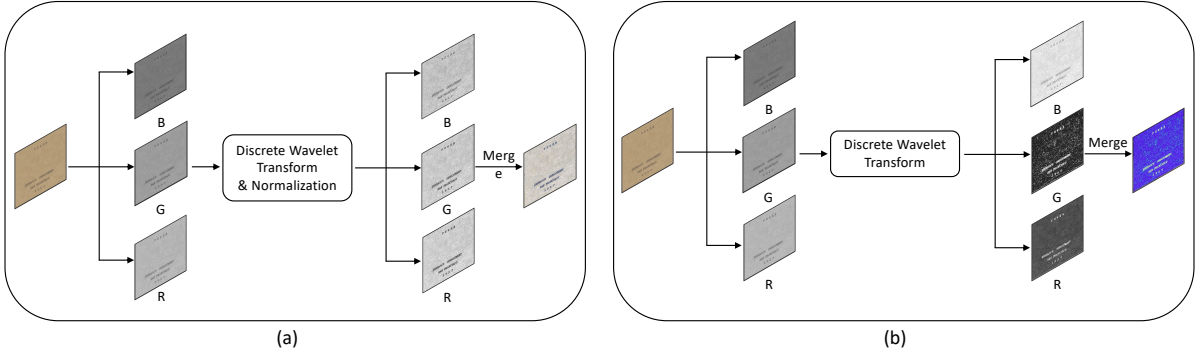


**Fig. 6** Example of normalizing the output image of HW15 in DIBCO 2011: (a) Normalization after DWT, (b) No normalization after DWT.

by the green component and the second document image is dominated by the blue component, which causes the dominance of the weight update to change continuously and the gradient update trajectory of the model becomes disordered and slow to converge, as shown in Fig. 5 (b).

We normalize the images of the LL subbands to make non-comparable data comparable, while maintaining the relative relationship between the two compared data. Fig. 6 demonstrates the effect of normalization on the images of RGB components after DWT. For the image HW15 in the DIBCO 2011 dataset, normalization handles the RGB component very well, while the output image without normalization is dominated by the blue component. The effect of normalization on the experimental results is described in detail in the comparison experiment in Section 4.5.

### 3.3 Stage-2

In Stage-2, the proposed method is shown in Fig. 7. We first split the input original image into four channels, each channel uses an independent generator and all channels share a common discriminator for distinguishing the generated image from the corresponding ground truth image. The four generators are trained using images from the red, green, blue, and gray channels, respectively. The trained adversarial networks can remove the background information from the local image blocks and extract the colored foreground information.

#### 3.3.1 Network architecture

The generator uses an encoder-decoder architecture, where the generator uses U-Net++ [51] [52].

The encoders in the generator can extract features, and multiple decoders of different depths share a single encoder and are concatenated together. We use the skip connection mechanism between the encoder and multiple decoders. The encoder acts the role to downsample and extract context information, while the decoders perform upsampling and combine the features of upsampling with those of downsampling. The encoder is accomplished by using EfficientNet [46], which is a lightweight CNN with good performance in image classification tasks. We improve the discriminator in PatchGAN [22] [53] [21] as the discriminator of the network architecture due to better generalization.

Because the degradation of color documents cannot be predicted, four separate adversarial networks are used to extract the text information in different color backgrounds, which can reduce the color interference in the processing of document image binarization. The discriminator requires input images of the same channel, since the image generated by the generator consists of four channels (red, green, blue, and gray), while the ground truth image has only one channel (the grayscale image). We combine the three single-channel output images (red, green, and blue) from Stage-1 with the ground truth image, which satisfies the requirements of the input discriminator.

#### 3.3.2 Loss functions of GAN

To ensure a more stable convergence of the loss function, we apply Wasserstein GAN (WGAN-GP) [9] to the target function. Experiments by Bartusiak *et al.* [1] showed that the binary cross-entropy (BCE) loss has better performance than

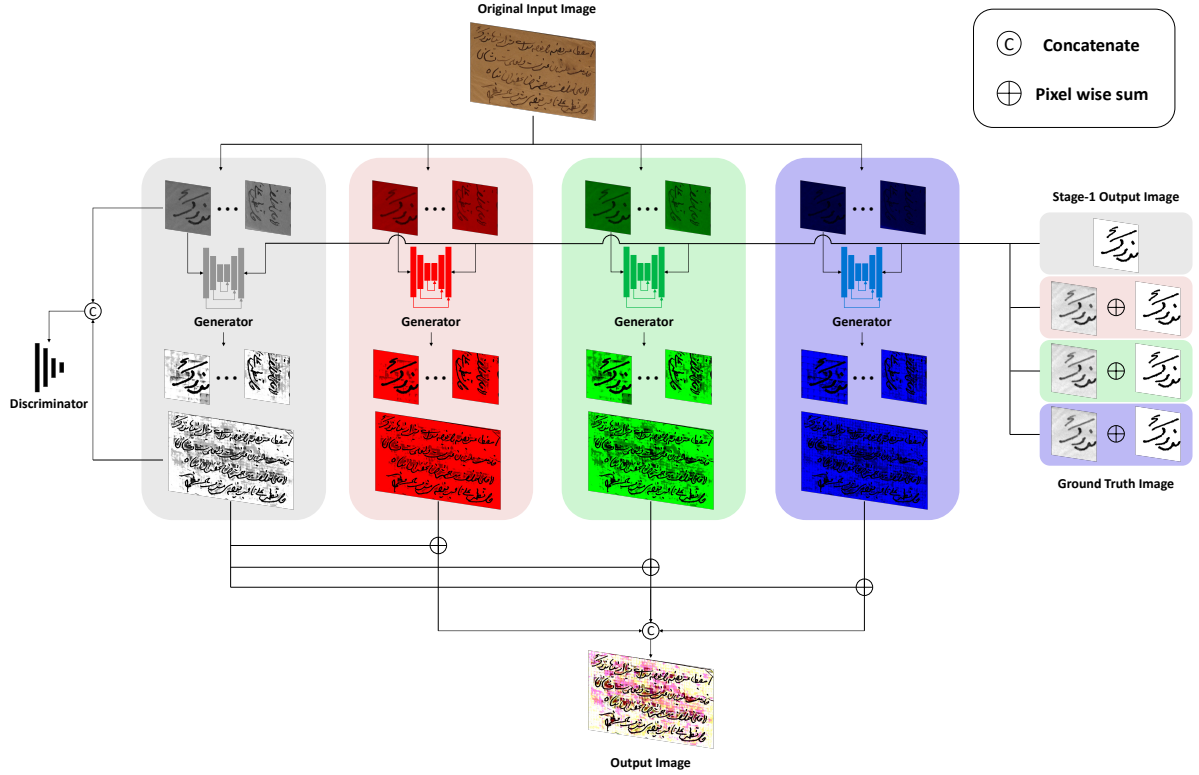


**Fig. 7** Flowchart of Stage-2 in our method.

the  $L1$  loss for binary classification, and therefore we use the BCE loss instead of the  $L1$  loss of Pix2Pix GAN [14]. The WAGN-GP target loss function including the BCE loss is formulated as follows:

$$\mathbb{L}_D = -\mathbb{E}_{x,y}[D(y, x)] + \mathbb{E}_x[D(G(x), x)] + \alpha \mathbb{E}_{x, \hat{y} \sim P_{\hat{y}}}[(\|\nabla_{\hat{y}} D(\hat{y}, x)\|_2 - 1)^2] \quad (6)$$

$$\mathbb{L}_G = \mathbb{E}_x[D(G(x), x)] + \lambda \mathbb{E}_{G(x), y}[y \log G(x) + (1 - y) \log(1 - G(x))] \quad (7)$$

where the penalty coefficient is  $\alpha$ , and the uniform sampling along a straight line between the ground truth distribution  $P_y$  and the point pairs of the generated data distribution is  $P_{\hat{y}}$ .  $\lambda$  is used to control the relative importance of different loss terms. The parameter of the generator is  $\theta_G$  and the parameter of the discriminator is  $\theta_D$ . In the discriminator, the generated image is distinguished from the real image by the target loss function  $\mathbb{L}_D$  in Eq. (6). In the generator, the distance between

the generated image and the ground truth image in each color channel is minimized by the target loss function  $\mathbb{L}_G$  in Eq. (7).

Algorithm 1 shows the detailed procedure to train the GAN models. The training process is based on the training environment we built, which includes the selection of the optimizer, the setting of the learning rate, and the setting of the loss function. As we can see from the algorithm, the GAN model continuously updates the loss function by the authenticity of the generated image through the discriminator, so that the generator can output a more realistic image.

### 3.4 Stage-3

Stage-3 uses a multi-scale adversarial network to generate images of local binarization results and global binarization results, respectively, which can distinguish the background part and text part more accurately. Unlike Stage-2 where the local prediction with small patches is mainly used, we perform global binarization on the original size of the input images in Stage-3 to compensate for the loss of contextual information of the text images

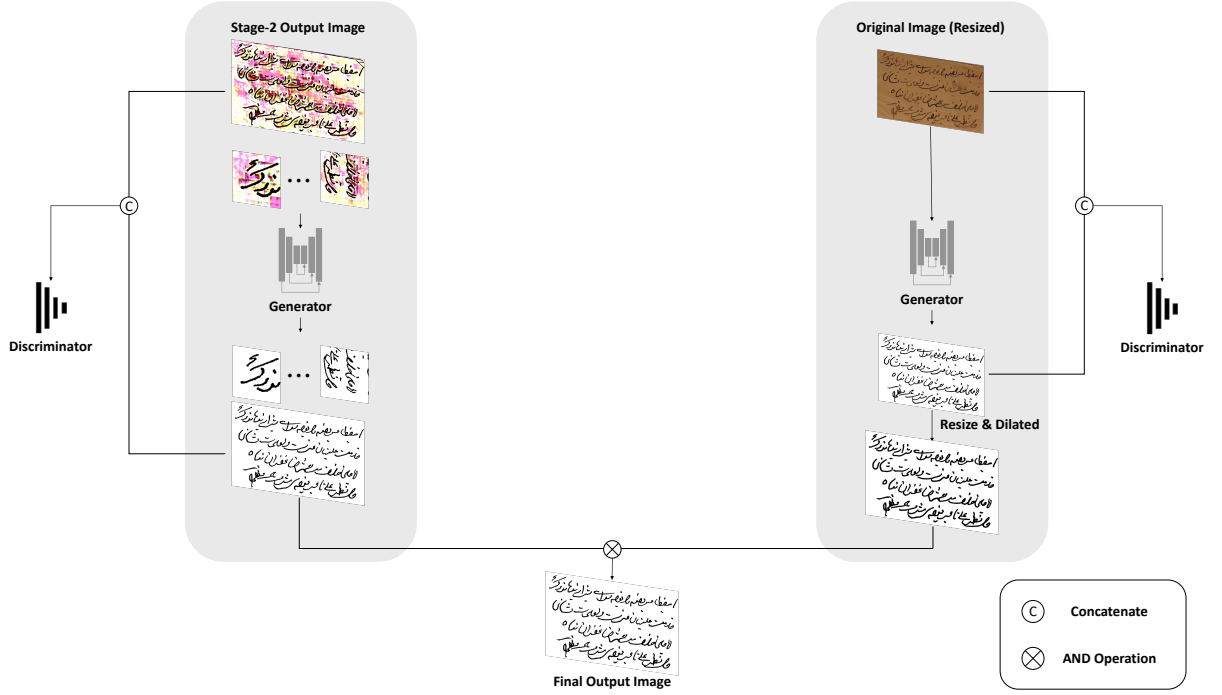


**Fig. 8** Flowchart of Stage-3 in our method.

**Algorithm 1** Training process for GAN using the output images of Stage-1

**Require:** Adam optimizer,  $\eta = 1 \times 10^{-4}$

**Ensure:**  $\omega = 0.5$ ,  $\alpha = 10$ ,  $\lambda = 50$

```

1: Initialize: Parameters  $\theta_{G_r}$ ,  $\theta_{G_g}$ ,  $\theta_{G_b}$ ,  $\theta_{G_{gray}}$ 
2: for number of training iterations do
3:   Input Image Split into  $r, g, b, gray$  images
4:   for  $k = \{r, g, b, gray\}$  do
5:     if  $k$  is gray then
6:        $y_k \leftarrow y$ 
7:     else
8:        $x'_k = \text{Norm}(V_{LL}(x_k))$ 
9:        $y_k \leftarrow x'_k \cap y$ 
10:      Binarize  $y_k$  with threshold value  $t$ .
11:    end if
12:    Update Discriminator  $D$  (Eq. (6)):
13:     $\theta_D \leftarrow \theta_D - \eta_D \nabla_{\theta_D} \mathbb{L}_D$ 
14:    Update Generator  $G_k$  (Eq. (7)):
15:     $\theta_{G_k} \leftarrow \theta_{G_k} - \eta_G \nabla_{\theta_{G_k}} \mathbb{L}_G$ 
16:  end for
17: end for
18: for  $k = \{r, g, b\}$  do
19:    $\hat{y}_k \leftarrow \omega G_k(x_k) + (1 - \omega) G_{gray}(x_{gray})$ 
20: end for
21:  $\hat{y} \leftarrow [\hat{y}_r, \hat{y}_g, \hat{y}_b]$ 

```

due to local prediction in the second stage. As shown in Fig. 8, two discriminators are employed in Stage-3 because the input image for the local prediction in Stage-2 is 8-bit images, while Stage-3 uses 24-bit three-channel images. In addition, the figure shows that the input image on the left side of the figure is small patches from the Stage-2 output for local prediction, while the input image on the right side of the figure is the original input image for global prediction.

For Stage-3 of the binarization process, the network architecture of the generator is the same as that of Stage-2 except for the number of input channels. For public datasets such as DIBCO, the provided document images contain images of various scales, and therefore in Stage-3 we directly binarize the original input images by resizing them to the desired size.

## 4 Experiments

### 4.1 Datasets

We compare the proposed method with several classical methods and SOTA methods on multiple public datasets. For the training set we selected the datasets DIBCO 2009 [7], H-DIBCO 2010 [32],



**Table 1** Comparison Experiment of Stage-1 on DIBCO 2011

Option	Input	GT	FM↑	p-FM↑	PSNR↑	DRD↓
1	\	\	86.68	89.61	19.27	4.01
2	\	DWT (LL)	88.20	90.57	19.53	3.45
3	\	DWT (LL) + Norm	87.70	90.24	19.65	3.45
4	DWT (LL)	\	87.74	89.69	18.88	3.78
5	DWT (LL) + Norm	\	89.33	91.94	19.49	3.37
6	DWT (LL)	DWT (LL)	<b>90.53</b>	<b>92.82</b>	<b>19.68</b>	<b>3.11</b>
7	DWT (LL) + Norm	DWT (LL) + Norm	89.06	92.25	19.59	3.31

**Table 2** Comparison Experiment of Stage-1 on DIBCO 2013

Option	Input	GT	FM↑	p-FM↑	PSNR↑	DRD↓
1	\	\	92.94	94.70	21.57	2.74
2	\	DWT (LL)	94.43	95.64	21.79	2.13
3	\	DWT (LL) + Norm	<b>94.88</b>	<b>96.19</b>	<b>22.32</b>	<b>1.95</b>
4	DWT (LL)	\	93.23	94.43	20.80	2.67
5	DWT (LL) + Norm	\	93.76	95.41	21.54	2.40
6	DWT (LL)	DWT (LL)	94.39	95.34	21.91	2.26
7	DWT (LL) + Norm	DWT (LL) + Norm	94.55	95.86	22.02	2.07

H-DIBCO 2012 [34], Persian Heritage Image Binarization Dataset (PHIBD) [25], Synchromedia Multispectral Ancient Document Images Dataset (SMADI) [12], and Bickley Diary Dataset [6]. Besides, datasets DIBCO 2011, DIBCO 2013, H-DIBCO 2014, H-DIBCO 2016, DIBCO 2017, and H-DIBCO2018 [28, 33, 35–38] are selected as test sets.

#### 4.1.1 DIBCO

DIBCO is the public dataset provided by Document Image Binarization Contest. There are nine datasets, DIBCO 2009, H-DIBCO 2010, DIBCO 2011, H-DIBCO 2012, DIBCO 2013, DIBCO 2017, H-DIBCO 2014, H-DIBCO 2016, and H-DIBCO 2018. These datasets contain both grayscale and color machine-printed and handwritten images. In the competition, participants were asked to design algorithms to extract binarized text images from handwritten and machine-printed images in the datasets.

#### 4.1.2 PHIBD

PHIBD is the Persian Heritage Image Binarization Dataset. This dataset contains 15 historical and old manuscript images from the historical records of Mirza Mohammad Kazemini’s old manuscript library in Yazd, Iran. The images in the dataset

have suffered from various types of degradation, including bleeding, fading, and blurring.

#### 4.1.3 SMADI

SMADI is the Synchromedia Multispectral Ancient Document Images Dataset. The dataset consists of 240 multispectral images of 30 authentic historical handwritten letters. All ancient manuscripts are written in iron gall ink and from the 17th to the 20th centuries. The original documents are deposited at the BAnQ Bibliothèque et Archives nationales du Québec. The dataset is imaged with a CROMA CX MSI camera, generating 8 images per document, for a total of 240 images of real documents captured, calibrated, and registered.

#### 4.1.4 Bickley Diary Dataset

Bickley Diary Dataset is donated to the Singapore Methodist Archives by Erin Bickley. The dataset consists of diaries where the images are affected by light and fold damage, making identification more difficult.

### 4.2 Evaluation Metric

In evaluating the different methods, we use four evaluation metrics, including F-measure (FM),

**Table 3** Comparison Experiment of Stage-1 on H-DIBCO 2014

Option	Input	GT	FM↑	p-FM↑	PSNR↑	DRD↓
1	\	\	96.50	97.50	22.08	1.01
2	\	DWT (LL)	96.52	97.70	22.15	0.99
3	\	DWT (LL) + Norm	<b>96.88</b>	<b>98.03</b>	<b>22.68</b>	<b>0.89</b>
4	DWT (LL)	\	95.94	96.91	21.31	1.19
5	DWT (LL) + Norm	\	96.29	97.48	22.05	1.16
6	DWT (LL)	DWT (LL)	96.60	97.60	22.27	0.97
7	DWT (LL) + Norm	DWT (LL) + Norm	96.77	97.89	22.52	0.91

**Table 4** Comparison Experiment of Stage-1 on H-DIBCO 2016

Option	Input	GT	FM↑	p-FM↑	PSNR↑	DRD↓
1	\	\	90.74	94.46	19.39	3.30
2	\	DWT (LL)	91.76	95.74	19.67	2.93
3	\	DWT (LL) + Norm	91.49	<b>96.46</b>	19.68	2.92
4	DWT (LL)	\	91.86	94.95	19.62	2.99
5	DWT (LL) + Norm	\	91.28	96.03	19.47	3.04
6	DWT (LL)	DWT (LL)	91.68	95.90	19.68	2.93
7	DWT (LL) + Norm	DWT (LL) + Norm	<b>91.95</b>	95.87	<b>19.75</b>	<b>2.84</b>

pseudo-F-measure (p-FM), peak signal-to-noise ratio (PSNR), and the distance reciprocal distortion (DRD).

- **F-measure (FM):**

$$\frac{2 \times Recall \times Precision}{Recall + Precision} \quad (8)$$

where  $Recall = \frac{TP}{TP+FN}$ ,  $Precision = \frac{TP}{TP+FP}$ , and  $TP$ ,  $FP$ , and  $FN$  denote the true positive, false positive, and false negative values, respectively.

- **Pseudo-F-measure (p-FM):**

$$\frac{2 \times Recall_{ps} \times Precision_{ps}}{Recall_{ps} + Precision_{ps}} \quad (9)$$

where Pseudo-Recall ( $Recall_{ps}$ ) and Pseudo-Precision ( $Precision_{ps}$ ) both use the distance weights relative to the ground truth image profile to generate a new weighted ground truth image.

- **Peak signal-to-noise ratio (PSNR):**

$$10 \log \left( \frac{V^2}{MSE} \right) \quad (10)$$

$$MSE = \frac{\sum_{x=1}^{width} \sum_{y=1}^{height} (L(x, y) - L'(x, y))^2}{width \times height} \quad (11)$$

where  $V$  is the difference between foreground and background.  $PSNR$  is a measure to detect the similarity between two images, and the larger the value of  $PSNR$ , the more similar the two images are.

- **Distance reciprocal distortion (DRD):**

$$\frac{\sum_k DRD_k}{NUBN} \quad (12)$$

$$DRD_k = \sum_{i=-2}^2 \sum_{j=-2}^2 |G_k(i, j) - B_k(x, y)| \times N_w(i, j) \quad (13)$$

where  $DRD$  is a measure of visual distortion in the binary image;  $NUBN$  is the number of uneven  $8 \times 8$  blocks in the ground truth image, and  $DRD_k$  is the distortion of the  $k_{th}$  flipped pixel calculated using a  $5 \times 5$  normalized weight matrix  $N_w$ .  $B_k$  denotes the pixel of the binary image and  $G_k$  denotes the pixel of the ground truth image.

**Table 5** Ablation study of the proposed method on several datasets.

Methods	Dataset	FM $\uparrow$	p-FM $\uparrow$	PSNR $\uparrow$	DRD $\downarrow$
Stage-2	DIBCO 2011	80.32	93.93	16.02	5.19
Proposed		94.08	97.08	20.51	1.75
Stage-2	DIBCO 2013	86.19	97.36	17.91	3.81
Proposed		95.24	97.51	22.27	1.59
Stage-2	H-DIBCO 2014	86.96	95.98	17.15	3.85
Proposed		96.65	98.19	22.27	0.96
Stage-2	H-DIBCO 2016	81.60	95.65	16.82	5.62
Proposed		91.46	96.32	19.66	2.94
Stage-2	DIBCO 2017	78.76	93.30	15.15	5.84
Proposed		90.95	93.79	18.57	2.94
Stage-2	H-DIBCO 2018	64.08	74.55	13.23	11.54
Proposed		91.66	95.53	20.02	2.81

### 4.3 Implementation Details

All experiments are implemented using Python in the PyTorch framework, and we use the NVIDIA RTX 3090 GPU for the training process.

#### 4.3.1 Training

In order to fairly compare the performance of all methods, we use the same data enhancement as our proposed method for both other traditional and SOTA methods. Due to the GPU memory limitation during training, we resize the input images in the training set into  $224 \times 224$  patches to train the network. The patches are sampled on the training dataset using scale factors of 0.75, 1.25, and 1.5 and rotate the images by  $270^\circ$ . Finally, we create around 150,000 training image patches from the dataset.

In Stage-3 of global binarization, we do not use zoom and rotate image enhancement; only horizontal flip is applied, and there are 804 training patches. The input of Stage-3 of local binarization is the output of Stage-2, and the parameters of Stage-2 and Stage-3 of training are set to the same. In addition to training 150 epochs globally, we train 10 epochs on all datasets for the other networks. Adam [17] is chosen as the optimizer and the learning rate is set to  $1 \times 10^{-4}$ ,  $\beta_1 = 0.5$  for the generator and  $\beta_2 = 0.999$  for the discriminator.

### 4.4 Comparison with other Methods

Our proposed method is evaluated in the DIBCO datasets, and the four evaluation metrics used are introduced in Section 4.2 to compare the different

methods, including the traditional binarization methods: Otsu [29], Niblack [26], and Sauvola [40], and the several SOTA methods: Vo *et al.* [48], He *et al.* [11], Souibgui *et al.* [41], Suh *et al.* [43], Kang *et al.* [16], Tensmeyer *et al.* [47], Souibgui *et al.* [41], Jemni *et al.* [15], Guo *et al.* [10], and Bera *et al.* [2]. In addition, for the datasets for which the Document Image Binarization Competition has provided competition data, we also include a comparison of the performance of the first place of the competition [28, 33, 35–38].

### 4.5 Comparison Experiment

In Stage-1, we perform DWT and normalization on the original input images. Although the mathematical theory demonstrates that the processed images can store contour information and reduce noise more efficiently, we would like to better understand the impact of the processed images on the experimental results.

In this section, a comparison experiment is conducted to find out that whether the output images from Stage-1 or the corresponding ground truth images as the Stage-2 input images would have better performance. We use UNet [39] as the generator to evaluate the network model on the datasets DIBCO 2011, DIBCO 2013, H-DIBCO 2014, and H-DIBCO 2016. For the input images of the generator, three options are set up: (1) direct input, (2) DWT to obtain LL subband, and (3) DWT to obtain LL subband followed by normalization. For the corresponding ground truth images of the generator, except for the ground truth channel (1-D), it sets three options for the



**Fig. 9** Example of images enhancement and binarization in the DIBCO dataset: (a) the original input image, (b) the LL subband image using discrete wavelet transformation and normalization (Stage-1), (c) the enhanced image using our image enhancement method (Stage-2), (d) the binarization image using our method combining local and global features (Stage-3), (e) the ground truth image.

images of the other three channels, which are used in the same way as the input images.

Tables 1, 2, 3, and 4 show the comparisons of all options and their model performances on the four datasets. On these four datasets, Option 1 that the generator directly inputs the original images and directly uses three channels of the original images and a single channel of ground truth images provides the worst performance. Table 1 shows that Option 6 using only DWT without normalization as the input image and corresponding ground truth image performs well on the DIBCO 2011 dataset. It can be seen in Tables 2 and 3 that Option 3 of directly inputting the original images and using Stage-1 output images as the

corresponding ground truth images provide the best performance on the DIBCO 2013 and H-DIBCO 2014 datasets. In addition, the model of Option 3 in Table 4 can obtain the highest p-FM value. Therefore, we choose Option 3 to build our network model architecture.

## 4.6 Ablation Study

In this section, we conduct an ablation study to verify the contribution of each stage to the network model in the whole architecture. We validate the output image of Stage-2 and name it “Stage-2”. The output image of Stage-3 is the final output

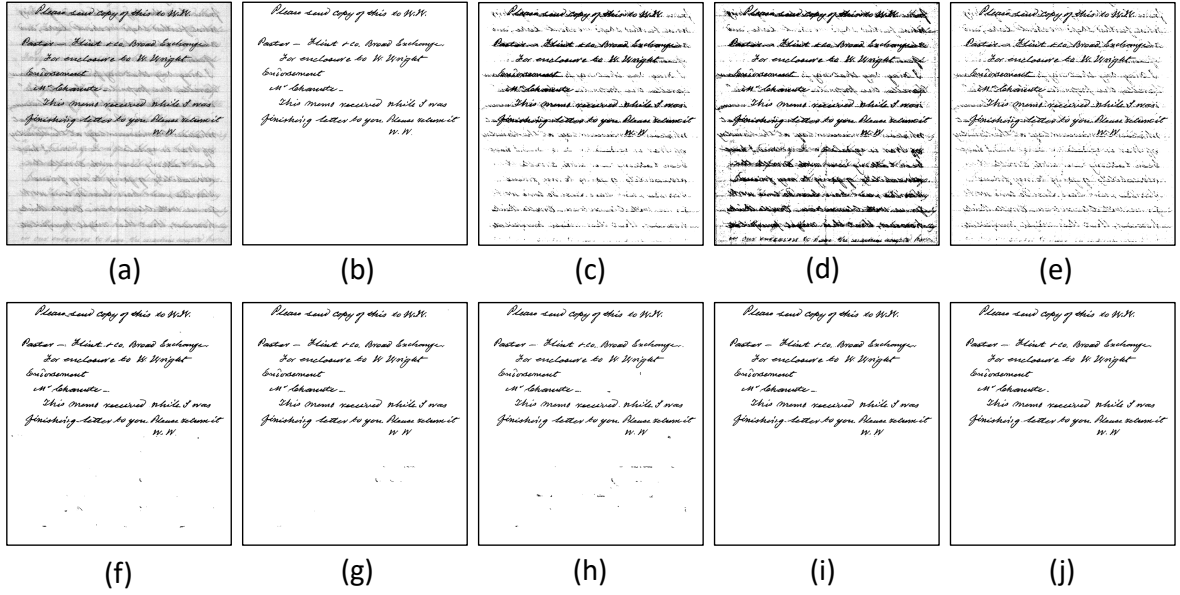


**Fig. 10** Document binarization results for the input image HW1 of DIBCO 2011 by different methods: (a) original input images, (b) the ground truth, (c) Otsu [29], (d) Niblack [26], (e) Sauvola [40], (f) Vo [48], (g) He [11], (h) Zhao [50], (i) Suh [43], (j) Ours.

image, which we call “Proposed”. The two methods were compared on several DIBCO datasets (DIBCO 2011, DIBCO 2013, H-DIBCO 2014, H-DIBCO 2016, DIBCO 2017 and H-DIBCO 2018). The results of the evaluation are shown in Table 5, where the Stage-2 outputs are worse than the final outputs in terms of FM, p-FM, PSNR and DRD.

In the comparison experiments of Section 4.5, it shows that training the generator after DWT and normalization of the images improves the performance of the network model. However, we would like to show the advantages of each stage better. It selects 5 images from PHIBD and Bickley Diary Dataset to show the output results of image enhancement and binarization using the proposed method step by step. As shown in Fig. 9, Fig. 9 (b) represents the result of retaining the LL subband images after DWT and normalization. This stage performs noise reduction on the original input image, which is used as the ground truth image for the generator. Fig. 9 (c) is the result of image enhancement using adversarial networks, where the image has had the background color removed and the color of the text highlighted. Fig. 9 (d) is the final output image obtained using the

**Table 6** Performance evaluation of different methods for document binarization on DIBCO 2011

Methods	FM↑	p-FM↑	PSNR↑	DRD↓
Niblack [26]	70.44	73.03	12.39	24.95
Otsu [29]	82.10	85.96	15.72	8.95
Sauvola [40]	82.35	88.63	15.75	7.86
He [11]	91.92	95.82	19.49	2.37
Vo [48]	92.58	94.67	19.16	2.38
Zhao [50]	92.62	95.38	19.58	2.55
Suh [43]	93.57	95.93	20.22	1.99
Tensmeyer [47]	93.60	<b>97.70</b>	20.11	1.85
Ours	<b>94.08</b>	97.08	<b>20.51</b>	<b>1.75</b>

**Table 7** Performance evaluation of different methods for document binarization on DIBCO 2013

Methods	FM↑	p-FM↑	PSNR↑	DRD↓
Niblack [26]	71.38	73.17	13.54	23.10
Otsu [29]	80.04	83.43	16.63	10.98
Sauvola [40]	82.73	88.37	16.98	7.34
Vo [48]	93.43	95.34	20.82	2.26
He [11]	93.36	96.70	20.88	2.15
Zhao [50]	93.86	96.47	21.53	2.32
1st Place [35]	92.12	94.19	20.68	3.10
Ours	<b>95.24</b>	<b>97.51</b>	<b>22.27</b>	<b>1.59</b>

proposed method, and it can be seen that our output results are close to the ground truth image as shown in Fig. 9 (e).



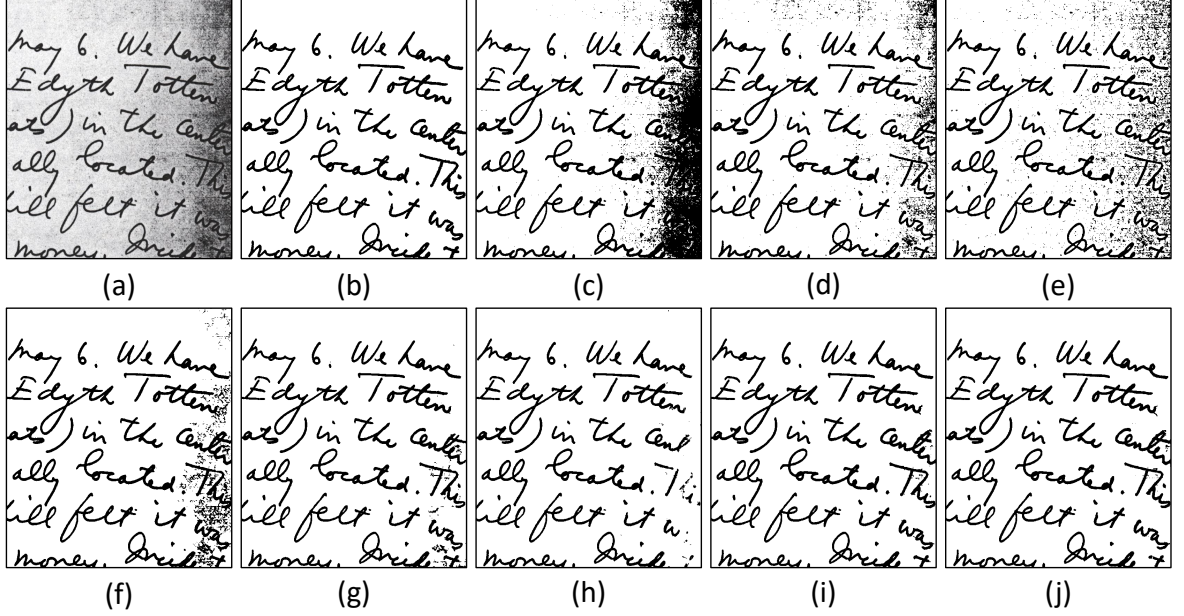


**Fig. 11** Document binarization results for the input image HW5 of DIBCO 2013 by different methods: (a) original input images, (b) the ground truth, (c) Otsu [29], (d) Niblack [26], (e) Sauvola [40], (f) Vo [48], (g) He [11], (h) Zhao [50], (i) Suh [43], (j) Ours.

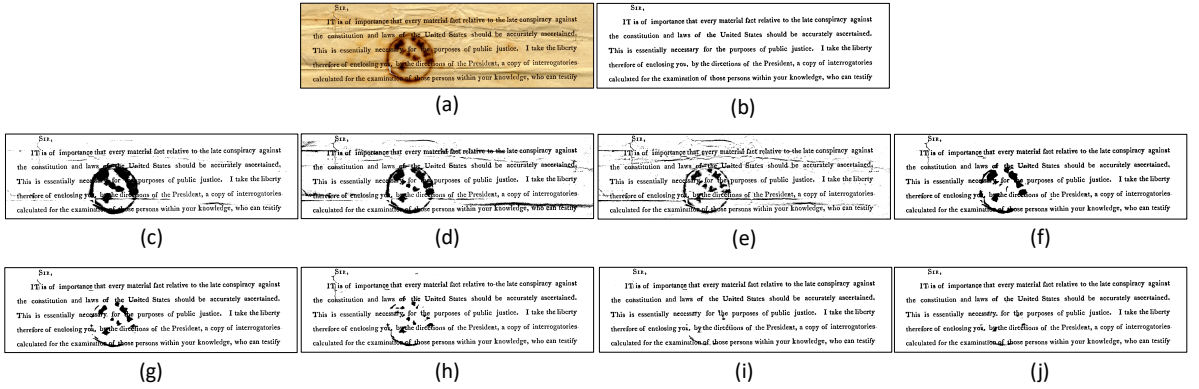


**Fig. 12** Document binarization results for the input image PR16 of DIBCO 2013 by different methods: (a) original input images, (b) the ground truth, (c) Otsu [29], (d) Niblack [26], (e) Sauvola [40], (f) Vo [48], (g) He [11], (h) Zhao [50], (i) Suh [43], (j) Ours.

## 4.7 Experimental Results

In this work, different models are evaluated on six DIBCO datasets (DIBCO 2011, DIBCO 2013, H-DIBCO 2014, H-DIBCO 2016, DIBCO 2017, and H-DIBCO 2018). Since the DIBCO datasets do not provide OCR output, this work uses the four evaluation metrics introduced in Section 4.2 to evaluate the proposed method and SOTA method.

Tables 6, 7, 8, 9, 10, and 11 show the results of the evaluation of the model on the six DIBCO datasets. On the DIBCO 2011 dataset (Table 6), the proposed method achieves the best performance in terms of FM, PSNR, and DRD, while the proposed method (97.08) is close to the best performance (97.70) in terms of p-FM. In the DIBCO 2013 dataset (Table 7), the proposed method achieves the best performance in all terms.

**Table 8** Performance evaluation of different methods for document binarization on H-DIBCO 2014

Methods	FM $\uparrow$	p-FM $\uparrow$	PSNR $\uparrow$	DRD $\downarrow$
Sauvola [40]	83.72	87.49	17.48	5.05
Niblack [26]	86.01	88.04	16.54	8.26
Otsu [29]	91.62	95.69	18.72	2.65
Vo [48]	95.97	97.42	21.49	1.09
He [11]	95.95	<b>98.76</b>	21.60	1.12
Zhao [50]	96.09	98.25	21.88	1.20
Suh [43]	96.36	97.87	21.96	1.07
1st Place [28]	<b>96.88</b>	97.65	<b>22.66</b>	<b>0.90</b>
Ours	96.65	98.19	22.27	0.96

**Table 9** Performance evaluation of different methods for document binarization on H-DIBCO 2016

Methods	FM $\uparrow$	p-FM $\uparrow$	PSNR $\uparrow$	DRD $\downarrow$
Niblack [26]	72.57	73.51	13.26	24.65
Sauvola [40]	84.27	89.10	17.15	6.09
Otsu [29]	86.59	89.92	17.79	5.58
1st Place [37]	87.61	91.28	18.11	5.21
Guo [10]	88.51	90.46	18.42	4.13
Zhao [50]	89.77	94.85	18.80	3.85
Vo [48]	90.01	93.44	18.74	3.91
Bera [2]	90.43	91.66	18.94	3.51
He [11]	91.19	95.74	19.51	3.02
Suh [43]	<b>92.24</b>	95.95	<b>19.93</b>	<b>2.77</b>
Ours	91.46	<b>96.32</b>	19.66	2.94

**Table 10** Performance evaluation of different methods for document binarization on DIBCO 2017

Methods	FM $\uparrow$	p-FM $\uparrow$	PSNR $\uparrow$	DRD $\downarrow$
Otsu [29]	77.73	77.89	13.85	15.54
Sauvola [40]	77.11	84.10	14.25	8.85
Bera [2]	83.38	89.43	15.45	6.71
Jemni [15]	89.80	89.95	17.45	4.03
Zhao [50]	90.73	92.58	17.83	3.58
1st Place [38]	91.04	92.86	18.28	3.40
Kang [16]	<b>91.57</b>	93.55	15.85	<b>2.92</b>
Ours	90.95	<b>93.79</b>	<b>18.57</b>	2.94

Besides, on the rest of the DIBCO datasets, the proposed method is able to rank in the top three in all terms. These results show that the proposed method is more effective than the SOTA method for binarization of degraded color documents.

We select images from DIBCO 2011 and DIBCO 2013 as examples of binarization results. Figs. 10, 11 and 12 show the binarization results of images HW1, HW5, and PR16 by different methods. It can be seen from the figures that the SOTA method is better than the traditional binarization method in removing shadows and noise, while the proposed method retains more text contents with better removal of shadows and noise.

**Table 11** Performance evaluation of different methods for document binarization on H-DIBCO 2018

Methods	FM $\uparrow$	p-FM $\uparrow$	PSNR $\uparrow$	DRD $\downarrow$
Otsu [29]	51.45	53.05	9.74	59.07
Sauvola [40]	67.81	74.08	13.78	17.69
Zhao [50]	87.73	90.60	18.37	4.58
1st Place [36]	88.34	90.24	19.11	4.92
Kang [16]	89.71	91.62	19.39	2.51
Souibgui [41]	89.21	92.54	19.47	3.96
Jemni [15]	<b>92.41</b>	94.35	<b>20.18</b>	<b>2.60</b>
Ours	91.66	<b>95.53</b>	20.02	2.81

## 5 Conclusion

This paper proposes a new method for image enhancement and binarization of color document images. The proposed method is divided into three stages to solve the text degradation problem in color backgrounds using DWT and multi-scale adversarial networks. Our method takes the images of LL subband by DWT to remove the noises from the images as the corresponding ground truth images of the generator, trains independent networks using single-channel images from each of the four different colors, and then combines the local and global binary transformation networks to perform binarization. To the best of our knowledge, this is the first three-stage method based on traditional image processing and deep learning. The experimental results show that the performance of the network model trained using U-Net++ as the generator and PatchGAN as the discriminator outperforms the traditional and the SOTA performance.

Our proposed three-stage method is a general backbone method that can be trained with different wavelet transformations and neural networks. We note that models of the Transformer architecture have recently stood out in computer vision tasks. In future work, we intend to apply the attention mechanism to generators to obtain more efficient network models and advance the development of document image binarization.

## 6 Acknowledgments

This work was supported in part by the National Science and Technology Council, Taiwan, under Grant No. MOST111-2221-E032-021.

## 7 Declarations

### 7.1 Funding

This work was supported in part by the National Science and Technology Council, Taiwan, under Grant No. MOST111- 2221-E032-021.

### 7.2 Competing interests

The authors have no financial or proprietary interests in any material discussed in this article.

### 7.3 Ethics approval

This research does not involve human participants and/or animals.

## References

- [1] Bartusiak, E.R., Yarlagadda, S.K., Güera, D., Bestagini, P., Tubaro, S., Zhu, F.M., Delp, E.J.: Splicing detection and localization in satellite imagery using conditional gans. In: 2019 IEEE Conference on Multimedia Information Processing and Retrieval (MIPR), pp. 91–96. IEEE (2019)
- [2] Bera, S.K., Ghosh, S., Bhowmik, S., Sarkar, R., Nasipuri, M.: A non-parametric binarization method based on ensemble of clustering algorithms. *Multimedia Tools and Applications* **80**(5), 7653–7673 (2021)
- [3] Bhunia, A.K., Bhunia, A.K., Sain, A., Roy, P.P.: Improving document binarization via adversarial noise-texture augmentation. In: 2019 IEEE International Conference on Image Processing (ICIP), pp. 2721–2725. IEEE (2019)
- [4] Calvo-Zaragoza, J., Gallego, A.J.: A selectional auto-encoder approach for document image binarization. *Pattern Recognition* **86**, 37–47 (2019)
- [5] De, R., Chakraborty, A., Sarkar, R.: Document image binarization using dual discriminator generative adversarial networks. *IEEE Signal Processing Letters* **27**, 1090–1094 (2020)
- [6] Deng, F., Wu, Z., Lu, Z., Brown, M.S.: Binarizationshop: a user-assisted software suite for converting old documents to black-and-white. In: Proceedings of the 10th annual joint conference on Digital libraries, pp. 255–258 (2010)
- [7] Gatos, B., Ntirogiannis, K., Pratikakis, I.: Icdar 2009 document image binarization contest (dibco 2009). In: 2009 10th International conference on document analysis and recognition, pp. 1375–1382. IEEE (2009)
- [8] Goodfellow, I., Pouget-Abadie, J., Mirza, M., Xu, B., Warde-Farley, D., Ozair, S., Courville, A., Bengio, Y.: Generative adversarial networks. *Communications of the ACM* **63**(11), 139–144 (2020)
- [9] Gulrajani, I., Ahmed, F., Arjovsky, M., Dumoulin, V., Courville, A.C.: Improved training of wasserstein gans. *Advances in neural information processing systems* **30** (2017)
- [10] Guo, J., He, C., Zhang, X.: Nonlinear edge-preserving diffusion with adaptive source for document images binarization. *Applied Mathematics and Computation* **351**, 8–22 (2019)
- [11] He, S., Schomaker, L.: Deepotsu: Document enhancement and binarization using iterative deep learning. *Pattern recognition* **91**, 379–390 (2019)
- [12] Hedjam, R., Cheriet, M.: Historical document image restoration using multispectral imaging system. *Pattern Recognition* **46**(8), 2297–2312 (2013)
- [13] Hsia, C.H., Lin, T.Y., Chiang, J.S.: An adaptive binarization method for cost-efficient document image system in wavelet domain. *Journal of Imaging Science and Technology* **64**(3), 30,401–1 (2020)
- [14] Isola, P., Zhu, J.Y., Zhou, T., Efros, A.A.: Image-to-image translation with conditional adversarial networks. In: Proceedings of the IEEE conference on computer vision and pattern recognition, pp. 1125–1134 (2017)

- [15] Jemni, S.K., Souibgui, M.A., Kessentini, Y., Fornés, A.: Enhance to read better: a multi-task adversarial network for handwritten document image enhancement. *Pattern Recognition* **123**, 108,370 (2022)
- [16] Kang, S., Iwana, B.K., Uchida, S.: Complex image processing with less data—document image binarization by integrating multiple pre-trained u-net modules. *Pattern Recognition* **109**, 107,577 (2021)
- [17] Kingma, D.P., Ba, J.: Adam: A method for stochastic optimization. *arXiv preprint arXiv:1412.6980* (2014)
- [18] Kligler, N., Katz, S., Tal, A.: Document enhancement using visibility detection. In: *Proceedings of the IEEE Conference on Computer Vision and Pattern Recognition*, pp. 2374–2382 (2018)
- [19] Konwer, A., Bhunia, A.K., Bhowmick, A., Bhunia, A.K., Banerjee, P., Roy, P.P., Pal, U.: Staff line removal using generative adversarial networks. In: *2018 24th International Conference on Pattern Recognition (ICPR)*, pp. 1103–1108. IEEE (2018)
- [20] Krizhevsky, A., Sutskever, I., Hinton, G.E.: Imagenet classification with deep convolutional neural networks. *Communications of the ACM* **60**(6), 84–90 (2017)
- [21] Ledig, C., Theis, L., Huszár, F., Caballero, J., Cunningham, A., Acosta, A., Aitken, A., Tejani, A., Totz, J., Wang, Z., et al.: Photo-realistic single image super-resolution using a generative adversarial network. In: *Proceedings of the IEEE conference on computer vision and pattern recognition*, pp. 4681–4690 (2017)
- [22] Li, C., Wand, M.: Precomputed real-time texture synthesis with markovian generative adversarial networks. In: *European conference on computer vision*, pp. 702–716. Springer (2016)
- [23] Long, J., Shelhamer, E., Darrell, T.: Fully convolutional networks for semantic segmentation. In: *Proceedings of the IEEE conference on computer vision and pattern recognition*, pp. 3431–3440 (2015)
- [24] Mirza, M., Osindero, S.: Conditional generative adversarial nets. *arXiv preprint arXiv:1411.1784* (2014)
- [25] Nafchi, H.Z., Ayatollahi, S.M., Moghaddam, R.F., Cheriet, M.: An efficient ground truthing tool for binarization of historical manuscripts. In: *2013 12th International Conference on Document Analysis and Recognition*, pp. 807–811. IEEE (2013)
- [26] Niblack, W.: *An introduction to digital image processing*. Strandberg Publishing Company (1985)
- [27] Nicolaou, A., Christlein, V., Riba, E., Shi, J., Vogeler, G., Seuret, M.: Tormentor: Deterministic dynamic-path, data augmentations with fractals. In: *Proceedings of the IEEE/CVF Conference on Computer Vision and Pattern Recognition*, pp. 2707–2711 (2022)
- [28] Ntirogiannis, K., Gatos, B., Pratikakis, I.: Icfhr2014 competition on handwritten document image binarization (h-dibco 2014). In: *2014 14th International conference on frontiers in handwriting recognition*, pp. 809–813. IEEE (2014)
- [29] Otsu, N.: A threshold selection method from gray-level histograms. *IEEE transactions on systems, man, and cybernetics* **9**(1), 62–66 (1979)
- [30] Peng, X., Cao, H., Natarajan, P.: Using convolutional encoder-decoder for document image binarization. In: *2017 14th IAPR international conference on document analysis and recognition (ICDAR)*, vol. 1, pp. 708–713. IEEE (2017)
- [31] Peng, X., Cao, H., Subramanian, K., Prasad, R., Natarajan, P.: Exploiting stroke orientation for crf based binarization of historical

- documents. In: 2013 12th International Conference on Document Analysis and Recognition, pp. 1034–1038. IEEE (2013)
- [32] Pratikakis, I., Gatos, B., Ntirogiannis, K.: H-dibco 2010-handwritten document image binarization competition. In: 2010 12th International Conference on Frontiers in Handwriting Recognition, pp. 727–732. IEEE (2010)
- [33] Pratikakis, I., Gatos, B., Ntirogiannis, K.: Icdar 2011 document image binarization contest (dibco 2011). In: 2011 International Conference on Document Analysis and Recognition, pp. 1506–1510. IEEE (2011)
- [34] Pratikakis, I., Gatos, B., Ntirogiannis, K.: Icfhr 2012 competition on handwritten document image binarization (h-dibco 2012). In: 2012 international conference on frontiers in handwriting recognition, pp. 817–822. IEEE (2012)
- [35] Pratikakis, I., Gatos, B., Ntirogiannis, K.: Icdar 2013 document image binarization contest (dibco 2013). In: 2013 12th International Conference on Document Analysis and Recognition, pp. 1471–1476. IEEE (2013)
- [36] Pratikakis, I., Zagori, K., Kaddas, P., Gatos, B.: Icfhr 2018 competition on handwritten document image binarization (h-dibco 2018). In: 2018 16th International Conference on Frontiers in Handwriting Recognition (ICFHR), pp. 489–493. IEEE (2018)
- [37] Pratikakis, I., Zagoris, K., Barlas, G., Gatos, B.: Icfhr2016 handwritten document image binarization contest (h-dibco 2016). In: 2016 15th International Conference on Frontiers in Handwriting Recognition (ICFHR), pp. 619–623. IEEE (2016)
- [38] Pratikakis, I., Zagoris, K., Barlas, G., Gatos, B.: Icdar2017 competition on document image binarization (dibco 2017). In: 2017 14th IAPR International Conference on Document Analysis and Recognition (ICDAR), vol. 1, pp. 1395–1403. IEEE (2017)
- [39] Ronneberger, O., Fischer, P., Brox, T.: U-net: Convolutional networks for biomedical image segmentation. In: International Conference on Medical image computing and computer-assisted intervention, pp. 234–241. Springer (2015)
- [40] Sauvola, J., Pietikäinen, M.: Adaptive document image binarization. *Pattern recognition* **33**(2), 225–236 (2000)
- [41] Souibgui, M.A., Biswas, S., Jemni, S.K., Kessentini, Y., Fornés, A., Lladós, J., Pal, U.: Docentr: An end-to-end document image enhancement transformer. *arXiv preprint arXiv:2201.10252* (2022)
- [42] Suh, S., Kim, J., Lukowicz, P., Lee, Y.O.: Two-stage generative adversarial networks for document image binarization with color noise and background removal. *arXiv preprint arXiv:2010.10103* (2020)
- [43] Suh, S., Lee, H., Lukowicz, P., Lee, Y.O.: Cegan: Classification enhancement generative adversarial networks for unraveling data imbalance problems. *Neural Networks* **133**, 69–86 (2021)
- [44] Sulaiman, A., Omar, K., Nasrudin, M.F.: Degraded historical document binarization: A review on issues, challenges, techniques, and future directions. *Journal of Imaging* **5**(4), 48 (2019)
- [45] Sun, B., Li, S., Zhang, X.P., Sun, J.: Blind bleed-through removal for scanned historical document image with conditional random fields. *IEEE Transactions on Image Processing* **25**(12), 5702–5712 (2016)
- [46] Tan, M., Le, Q.: Efficientnet: Rethinking model scaling for convolutional neural networks. In: International conference on machine learning, pp. 6105–6114. PMLR (2019)
- [47] Tensmeyer, C., Martinez, T.: Document image binarization with fully convolutional neural networks. In: 2017 14th IAPR international conference on document analysis and recognition (ICDAR), vol. 1, pp. 99–104.



IEEE (2017)

- [48] Vo, Q.N., Kim, S.H., Yang, H.J., Lee, G.: Binarization of degraded document images based on hierarchical deep supervised network. *Pattern Recognition* **74**, 568–586 (2018)
- [49] Zeiler, M.D., Fergus, R.: Visualizing and understanding convolutional networks. In: *European conference on computer vision*, pp. 818–833. Springer (2014)
- [50] Zhao, J., Shi, C., Jia, F., Wang, Y., Xiao, B.: Document image binarization with cascaded generators of conditional generative adversarial networks. *Pattern Recognition* **96**, 106,968 (2019)
- [51] Zhou, Z., Rahman Siddiquee, M.M., Tajbakhsh, N., Liang, J.: Unet++: A nested u-net architecture for medical image segmentation. In: *Deep learning in medical image analysis and multimodal learning for clinical decision support*, pp. 3–11. Springer (2018)
- [52] Zhou, Z., Siddiquee, M.M.R., Tajbakhsh, N., Liang, J.: Unet++: Redesigning skip connections to exploit multiscale features in image segmentation. *IEEE transactions on medical imaging* **39**(6), 1856–1867 (2019)
- [53] Zhu, J.Y., Park, T., Isola, P., Efros, A.A.: Unpaired image-to-image translation using cycle-consistent adversarial networks. In: *Proceedings of the IEEE international conference on computer vision*, pp. 2223–2232 (2017)